

Research Paper

Imaging of Chemokine Receptor 4 Expression in Neuroendocrine Tumors – a Triple Tracer Comparative Approach

Rudolf A. Werner^{1, 2, 3*}, Alexander Weich^{4, 5*}, Takahiro Higuchi¹, Jan S. Schmid¹, Andreas Schirbel¹, Michael Lassmann¹, Vanessa Wild⁶, Martina Rudelius^{5, 6}, Theodor Kudlich⁴, Ken Herrmann⁷, Michael Scheurlen⁴, Andreas K. Buck¹, Saskia Kropf⁸, Hans-Jürgen Wester⁹, Constantin Lapa¹✉

1. Department of Nuclear Medicine, University Hospital Würzburg, Würzburg, Germany;
2. The Russell H. Morgan Department of Radiology and Radiological Science, Johns Hopkins University School of Medicine, Baltimore, MD, United States;
3. Else-Kröner-Forschungskolleg, Interdisciplinary Center for Clinical Research, University of Würzburg, Würzburg, Germany;
4. Department of Internal Medicine II, Gastroenterology, University Hospital Würzburg, Würzburg, Germany;
5. Comprehensive Cancer Center Mainfranken, University Hospital Würzburg, Würzburg, Germany;
6. Institute for Pathology, University of Würzburg, Würzburg, Germany;
7. Department of Nuclear Medicine, University Hospital Essen, Essen, Germany;
8. Scintomics GmbH, Fürstenfeldbruck, Germany;
9. Pharmaceutical Radiochemistry, Technische Universität München, Munich, Germany.

* Both authors contributed equally to this work.

✉ Corresponding author: Constantin Lapa, MD., Department of Nuclear Medicine, University Hospital Würzburg, Würzburg, Germany, Oberdürrbacher Str. 6, 97080 Würzburg, Germany phone: +49 931 201 35412, fax: +49 931 201 6 444 00 email: lapa_c@ukw.de

© Ivyspring International Publisher. This is an open access article distributed under the terms of the Creative Commons Attribution (CC BY-NC) license (<https://creativecommons.org/licenses/by-nc/4.0/>). See <http://ivyspring.com/terms> for full terms and conditions.

Received: 2016.12.14; Accepted: 2017.02.13; Published: 2017.04.05

Abstract

C-X-C motif chemokine receptor 4 (CXCR4) and somatostatin receptors (SSTR) are overexpressed in gastro-entero-pancreatic neuroendocrine tumors (GEP-NET). In this study, we aimed to elucidate the feasibility of non-invasive CXCR4 positron emission tomography/computed tomography (PET/CT) imaging in GEP-NET patients using [⁶⁸Ga]Pentixafor in comparison to ⁶⁸Ga-DOTA-D-Phe-Tyr3-octreotide ([⁶⁸Ga]DOTATOC) and ¹⁸F-fluorodeoxyglucose ([¹⁸F]FDG). Twelve patients with histologically proven GEP-NET (3xG1, 4xG2, 5xG3) underwent [⁶⁸Ga]DOTATOC, [¹⁸F]FDG, and [⁶⁸Ga]Pentixafor PET/CT for staging and planning of the therapeutic management. Scans were analyzed on a patient as well as on a lesion basis and compared to immunohistochemical staining patterns of CXCR4 and somatostatin receptors SSTR2a and SSTR5. [⁶⁸Ga]Pentixafor visualized tumor lesions in 6/12 subjects, whereas [¹⁸F]FDG revealed sites of disease in 10/12 and [⁶⁸Ga]DOTATOC in 11/12 patients, respectively. Regarding sensitivity, SSTR-directed PET was the superior imaging modality in all G1 and G2 NET. CXCR4-directed PET was negative in all G1 NET. In contrast, 50% of G2 and 80% of G3 patients exhibited [⁶⁸Ga]Pentixafor-positive tumor lesions. Whereas CXCR4 seems to play only a limited role in detecting well-differentiated NET, increasing receptor expression could be non-invasively observed with increasing tumor grade. Thus, [⁶⁸Ga]Pentixafor PET/CT might serve as non-invasive read-out for evaluating the possibility of CXCR4-directed endoradiotherapy in advanced dedifferentiated SSTR-negative tumors.

Key words: Neuroendocrine tumor, [⁶⁸Ga]Pentixafor, CXCR4, chemokine receptor, PET/CT, SSTR, DOTATOC, PRRT, peptide receptor radionuclide therapy.

Introduction

Gastro-entero-pancreatic neuroendocrine tumors (GEP-NET) comprise a heterogeneous group of neoplasms originating from the endocrine cells of the intestinal tract. On the basis of tumor grade (assessed by mitotic rate as well as Ki67 index), GEP-NET are histologically separated into well-differentiated tumors of low grade (G1),

intermediate grade (G2), and poorly differentiated high grade (G3) neuroendocrine tumors (NET) [1, 2]. Most likely due to improved staging sensitivity and shifts in pathological classification, a marked overall increase in NET incidence over the last 20 years from 2.1/100,000/year to 4.9/100,000/year with the most pronounced rise in G3 NET from 0.01 to

1.8/100,000/year was recently reported [3].

Treatment options for well-differentiated, somatostatin receptor (SSTR)-expressing NET including biological agents (e.g. somatostatin analogs), conventional as well as peptide receptor radionuclide therapy (PRRT) have distinctly improved survival over the last decade [4-6]. However, treatment with (radiolabeled) SSTR analogs is generally not useful for G3 tumors, which do not express these receptors in an appropriate frequency and magnitude [7]. As a consequence, treatment response in case of tumor dedifferentiation and subsequent loss of SSTR expression is still poor, especially after failure to 1st line platinum-based chemotherapy [8, 9]. Hence, new therapeutic strategies in this setting are urgently needed.

Overexpression of C-X-C motif chemokine receptor 4 (CXCR4) and its ligand stromal cell derived factor 1 α (SDF-1 α) has been shown to play a pivotal role in several types of cancer including NET [10-12]. Recently, *Wester* and coworkers developed the theranostic agents [⁶⁸Ga]Pentixafor and [¹⁷⁷Lu]/[⁹⁰Y]Pentixather for non-invasive assessment of CXCR4 expression and subsequent chemokine-directed endoradiotherapy (ERT) [13-23].

Given the limited treatment options in case of dedifferentiation, identification of robust receptor expression on the tumor cell surface might pave the way for CXCR4-targeted ERT in SSTR-negative patients. Therefore, we aimed to evaluate this theranostic approach in NET using [⁶⁸Ga]Pentixafor-PET/CT in comparison to [⁶⁸Ga]DOTATOC and [¹⁸F]fluorodeoxyglucose ([¹⁸F]FDG). Imaging findings were also correlated with histological receptor expression derived from tumor samples.

Material and Methods

[⁶⁸Ga]Pentixafor was administered on a compassionate use basis in compliance with §37 of the Declaration of Helsinki and The German Medicinal Products Act, AMG §13.2b. Routine staging or restaging examinations included [¹⁸F]FDG and SSTR-directed PET with [⁶⁸Ga]DOTATOC. All patients underwent imaging for clinical purposes and gave written and informed consent to the diagnostic procedures. The study was approved by the local institutional review board of Würzburg (IRB approval: 2016100701).

Patients

From July 2015 till August 2016, a total of 12 patients (10 male, 2 female, median age, 68 years, range, 48 - 82) suffering from histologically proven GEP-NET were included. At the time point of imaging, all patients had not received treatment for at

least 4 weeks. Except a single patient, all subjects presented with an Eastern Cooperative Oncology Group (ECOG)/ World Health Organization (WHO) performance status ≤ 2 [24].

Preparation of [⁶⁸Ga]Pentixafor, [⁶⁸Ga]DOTATOC and [¹⁸F]FDG

Synthesis of [⁶⁸Ga]Pentixafor was performed by means of a fully GMP compliant automated synthesizer (GRP, Scintomics, Germany) [18, 25]. [¹⁸F]FDG and [⁶⁸Ga]DOTATOC were prepared as previously described [26, 27].

PET Imaging

All PET/CT scans were performed on a dedicated PET/CT scanner (Siemens Biograph mCT 64; Siemens Medical Solutions, Germany) within a median of 8 days (range, 1-64). Before acquisition of [¹⁸F]FDG-PET, patients fasted for at least 6 h and blood glucose levels were <160 mg/dl. Prior to [⁶⁸Ga]DOTATOC and [⁶⁸Ga]Pentixafor scans, no fasting was necessary. Imaging was performed 60 minutes after injection of 57 to 140 MBq (median, 120 MBq) of [⁶⁸Ga]Pentixafor, 269 to 325 MBq (median, 300 MBq) of [¹⁸F]FDG and 46 to 181 MBq (median, 137 MBq) of [⁶⁸Ga]DOTATOC, respectively. Spiral CT with (dose modulation with a quality reference of 210 mAs, for [¹⁸F]FDG-PET/CT scans) or without (80mAs, 120 kV, 512 x 512 matrix, 5 mm slice thickness) intravenous contrast including a field of view from the base of the skull to the proximal thighs was acquired. Consecutively, PET emission data were acquired in three-dimensional mode with a 200 x 200 matrix with 2-3 min emission time per bed position. After decay and scatter correction, PET data were reconstructed iteratively with attenuation correction using the algorithm implemented by the manufacturer (Siemens Esoft, Siemens, Erlangen, Germany).

Image Analysis

All PET scans were first visually rated by three experienced nuclear medicine physicians (CL, RAW, JSS) in a binary fashion as positive or negative for disease. Lesions were visually determined as focally increased tracer retention as compared to surrounding normal tissue or normal contralateral structures. Presence and number of metastases as well as location of lesions (up to 50 lesions per system ([nodal and/or hematogenous metastases]) were recorded.

Semi-quantitative analysis was performed for the primary tumor (if present) as well as the hottest metastatic lymph node and organ lesion, respectively. The axial PET image slice displaying the maximum tumor uptake was selected by drawing a 3D-volume

of interest (VOI) around the whole tumor area. Tumor regions of interest (ROIs) were defined in 2 ways. First, a standardized 10-mm circular region was placed over the area with the peak activity. This first ROI was used to derive maximum (SUV_{max}) and mean (SUV_{mean}) standardized uptake values. A reference bloodpool region was defined by drawing a ROI (diameter of 20 mm) in the left ventricle of the heart to derive tumor-to-background ratios (TBR). TBR for SUV_{max} and SUV_{mean} of all three tracers were calculated analyzing the primary (if still present), the hottest lymph node (LN) as well as visceral metastasis (M): $Primary_{max}/Background_{mean}$ (P_{max}/B_{mean}) and $Primary_{mean}/Background_{mean}$ (P_{mean}/B_{mean}); $LN_{max}/Background_{mean}$ (LN_{max}/B_{mean}) and $LN_{mean}/Background_{mean}$ (LN_{mean}/B_{mean}); $M_{max}/Background_{mean}$ (M_{max}/B_{mean}) and $M_{mean}/Background_{mean}$ (M_{mean}/B_{mean}). The radiotracer concentration in the ROIs was normalized to the injected dose per kilogram of patient's body weight to derive the SUVs.

Histological characterization of tumors

Immunohistochemistry was carried out on 10% formalin fixed paraffin embedded tissue sections ($3\mu m$) according to established protocols and scored as previously described [28]. CXCR4-immunohistochemistry was performed using an anti-CXCR4 rabbit polyclonal antibody (ab2074; Abcam, Cambridge, United Kingdom) followed by detection with the DAKO en vision system according to the manufacturer's protocol.

For assessment of SSTR expression, polyclonal antibodies against SSTR2a (1:500, RBK 046-05, Zytomed, Berlin, Germany) and SSTR5 (1:500, RBK 051-05, Zytomed, Berlin, Germany) were used. Samples from normal pancreatic tissue were used as positive control (islet cells). Dewaxed samples were pretreated with citrate buffer pH 6.0 for 10 minutes (for SSTR2a staining) or with the antigen retrieval agent TIRS-EDTA pH 9.0, respectively, for 10 minutes in a high pressure cooker (for SSTR5 staining). All immunostained sections were counterstained for 3 minutes with hematoxylin. The analysis of the stained sections was done semi-quantitatively by light-microscopy according to the immunoreactive score (IRS) by *Remmele* and *Stegner* [29]. The percentage of CXCR4-/SSTR-positive cells was scored as follows: 0 (no positive cells), 1 (<10% positive cells), 2 (10-50% positive cells), 3 (>50-80% positive cells), 4 (>80% positive cells). Additionally, the intensity of staining was graded: 0 (no color reaction), 1 (mild

reaction), 2 (moderate reaction), 3 (intense reaction). Multiplication of both scores for a given sample yields the IRS classification: 0-1 (negative), 2-3 (mild), 4-8 (moderate), 9-12 (strongly positive).

Statistical Analysis

All results are displayed as mean \pm SD or as median + range where appropriate.

Results

Clinical findings

4/12 patients suffered from ileum NET, 3/12 from pancreatic NET, 2/12 from gastric NET, and 1/12 from rectum NET, esophageal NET and mixed adenoneuroendocrine carcinoma (MANEC, neuroendocrine component > 60%) of the colon, respectively. At the time point of imaging, 4/12 subjects presented with newly diagnosed disease, the remainder (8/12) had already undergone various therapies including surgery (3/12), somatostatin analogs (3/12), conventional chemotherapy (3/12; 2/3, streptozocin/5-fluorouracil; 1/3, carboplatin/etoposide), peptide receptor radionuclide therapy (1/12) and transarterial chemoembolization (1/12).

The primary tumor was still present in 9/12 (75%) subjects. 11/12 patients presented with metastatic disease. Metastatic sites included liver (8/12), lymph nodes (LN; 7/12), bone (2/12), peritoneum (2/12), soft tissue (1/12) and lung (1/12).

Proliferation index Ki67 ranged from 1-90% with a median of 10%. According to the ENETS, AJCC, and the 2010 WHO classification, 3/12 cases could be classified as G1, 4/12 as G2 and 5/12 as G3 NETs [30-32]. Of note, all G3 NETs presented with a Ki67 index \geq 60%.

Clinical characteristics of the patient cohort are given in Table 1.

Imaging results of the whole cohort

On a patient basis, [^{68}Ga]Pentixafor was visually rated positive in 6/12 subjects (50%), whereas [^{18}F]FDG revealed sites of disease in 10/12 (83.3%) and [^{68}Ga]DOTATOC in 11/12 patients (91.7%), respectively (Figure 1A).

On a lesion basis, [^{68}Ga]Pentixafor detected a total of 69 lesions (5 primary tumors, 22 LN, 1 bone, 41 liver metastases) as opposed to 127 (5 primary tumors, 60 LN, 1 bone, 61 liver metastases) for [^{18}F]FDG and 245 (5 primary tumors, 151 liver, 51 bone, 33 LN, 4 peritoneal metastases, 1 soft tissue metastasis) for [^{68}Ga]DOTATOC.

Table 1. Detailed patient characteristics

CLINICAL DATA							PET				Histology/ IHC					
Case	Sex	Age (y)	Primary	WHO/ ECOG status*	Metastatic sites	Prior therapy	Ki67 (%)	WHO Grade	[⁶⁸ Ga] DOTATOC PET	[¹⁸ F] FDG PET	[⁶⁸ Ga] Pentixafor PET	Bx to PET (d)	Site of Bx	CXCR4 IRS	SSTR2 IRS	SSTR5 IRS
#1	m	76	gastric	0	liver	CTx	60	3	-	+	-	32	liver	0	0	1
#2	m	68	ileum	0	liver, LN	SSA	10	2	+	+	+	218	liver	0	12	0
#3	m	67	pancreatic	0	LN	none	85	3	+	+	+	18	pancreas	9	12	3
#4	f	48	pancreatic	0	liver	SSA, CTx, PRRT	10	2	+	+	+	930	pancreas	2	12	0
#5	m	82	ileum	0	liver	SSA, TAE	5	2	+	+	-	389	liver	0	12	4
#6	m	65	pancreatic	2	none	CTx	8	2	+	-	-	251	pancreas	0	12	2
#7	m	80	ileum	2	LN, liver, peritoneum	surgery	2	1	+	+	-	8	liver	0	12	12
#8	m	55	esophageal	3	LN, liver, bone	none	90	3	+	+	+	20	esophagus	2	0	0
#9	m	76	rectum	1	LN, liver, bone, soft tissue	none	2	1	+	+	-	89	rectum	1	9	3
#10	m	74	ileum	1	peritoneum	surgery	1	1	+	-	-	68	Ileum	0	8	4
#11	m	67	gastric	2	LN, liver, lung	none	90	3	+	+	+	18	stomach	2	0	12
#12	f	67	colon (MANEC)*	2	LN	surgery	90	3	+	+	+	49	colon	0	0	12

Bx = biopsy, CTx = chemotherapy, d = days, DOTATOC = DOTA-D-Phe-Tyr3-octreotide, ECOG = Eastern Cooperative Oncology Group, FDG = fluorodeoxyglucose, f = female, IRS = immunoreactive score, LN = lymph node, m = male, MANEC = mixed adenoneuroendocrine carcinoma, PET = positron emission tomography, PRRT = peptide receptor radionuclide therapy, SSA = somatostatin analog, TAE = transarterial embolization, WHO = World Health Organization, y = years. * neuroendocrine component of >60%

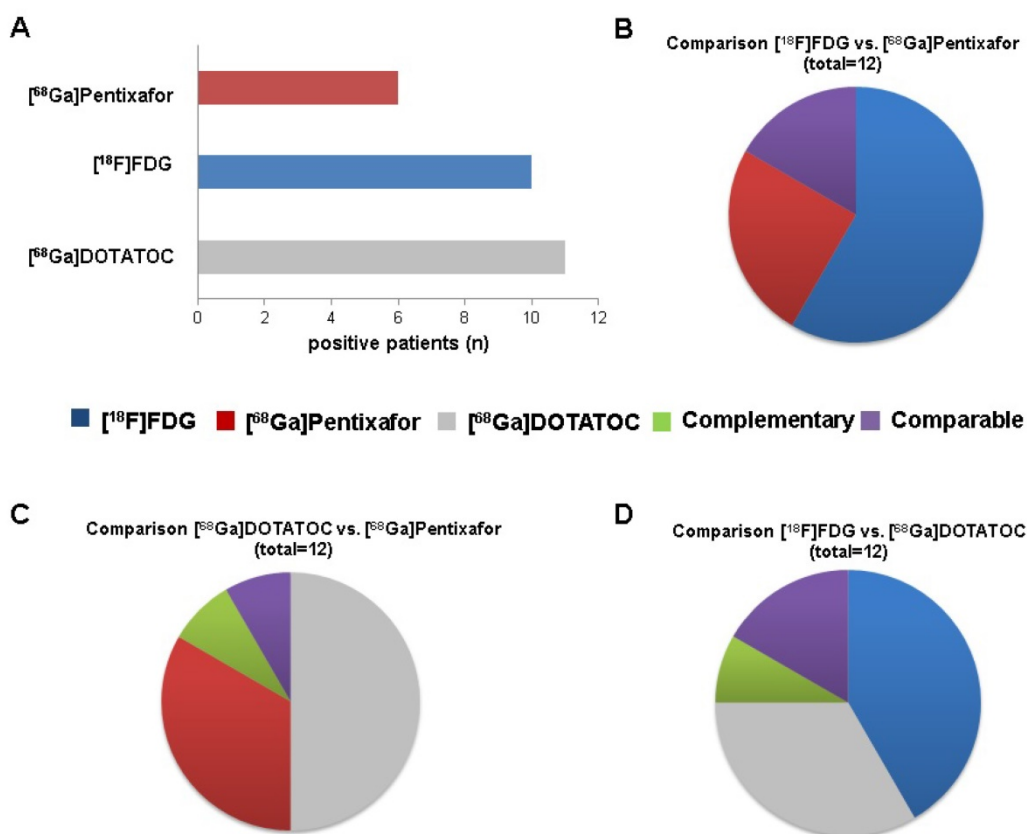


Figure 1. Visual comparison of [⁶⁸Ga]Pentixafor, ⁶⁸Ga-DOTA-D-Phe-Tyr3-octreotide ([⁶⁸Ga]DOTATOC) and ¹⁸F-fluorodeoxy-glucose ([¹⁸F]FDG) PET scans (whole cohort). The individual tracer's superiority over another was defined on a per-lesion basis, i.e. the tracer depicting the highest number of tumor lesions was considered superior. Comparability of two tracers was present when both detected the same number of identical lesions. Complementarity was defined of presence of sites of disease exclusively detected by one of the two compared tracers, respectively. **A.** Number of patients with visual positivity for the indicated PET tracer (total, n=12). **B.** Number of patients (total, n=12) for whom imaging with [¹⁸F]FDG (n=7) or [⁶⁸Ga]Pentixafor (n=3) was superior, with comparable positive findings (comparable, n=2) and with dual imaging providing no complementary information (complementary, n=0). **C.** Number of patients (total, n=12) for whom imaging with [⁶⁸Ga]DOTATOC (n=6) or [⁶⁸Ga]Pentixafor (n=4) was superior, with dual imaging providing complementary and comparable visual information in a single case each (complementary, n=1; comparable, n=1). **D.** Number of patients (total, n=12) for whom imaging with [¹⁸F]FDG (n=5) or [⁶⁸Ga]DOTATOC (n=4) was superior, with comparable positive findings (comparable, n=2) and with dual imaging providing complementary visual information (complementary, n=1).

Table 2. Display of mean (SUV_{mean}) and maximum (SUV_{max}) standardized uptake values (and corresponding median) for [⁶⁸Ga]Pentixafor, ⁶⁸Ga-DOTA-D-Phe-Tyr3-octreotide ([⁶⁸Ga]DOTATOC) and ¹⁸F-fluorodeoxy-glucose ([¹⁸F]FDG).

Grade	Ki67(%)	Patient	[⁶⁸ Ga]DOTATOC				[¹⁸ F]FDG				[⁶⁸ Ga]Pentixafor									
			P _{max}	P _{mean}	LN _{max}	LN _{mean}	M _{max}	M _{mean}	P _{max}	P _{mean}	LN _{max}	LN _{mean}	M _{max}	M _{mean}	P _{max}	P _{mean}	LN _{max}	LN _{mean}	M _{max}	M _{mean}
1	1	#10	-	-	-	-	14.3	12.9	-	-	-	-	-	-	-	-	-	-	-	-
1	2	#7	-	-	73.9	60.8	-	-	-	-	6.9	4.9	-	-	-	-	-	-	-	
1	2	#9	-	-	-	-	60.9	44.1	-	-	-	-	9.1	6.5	-	-	-	-	-	
Median of G1 NET			-	-	73.9	60.8	37.6	28.5	-	-	6.9	4.9	9.1	6.5	-	-	-	-	-	
2	5	#5	-	-	-	-	20	19.4	-	-	-	-	9	7	-	-	-	-	-	
2	8	#6	41	31.2	-	-	-	-	-	-	-	-	-	-	-	-	-	-	-	
2	10	#2	19.8	13.8	25.8	20.4	31.2	16.8	4.8	3.8	5.9	4.7	4.5	4.1	6.4	3.8	-	-	-	
2	10	#4	87.8	55.1	-	-	44.6	40.4	36.8	29.8	-	-	43.6	36.7	8.7	5.2	-	-	8.6	
Median of G2 NET			41	31.2	25.8	20.4	37.9	28.6	20.8	16.8	5.9	4.7	24.1	20.4	7.6	4.5	-	-	8.6	
3	60	#1	-	-	-	-	-	-	-	-	-	-	15	12.7	-	-	-	-	-	
3	85	#3	15.5	9.7	13.7	8.3	-	-	6.5	5.3	-	-	-	-	10.2	6	9.7	5.8	-	
3	90	#8	-	-	-	-	8	5.5	17.2	6.3	10.8	10	20.7	9.6	7.2	3.7	9.3	4.3	10.5	
3	90	#11	30.5	21.9	-	-	-	-	9.2	5.2	4.3	3.3	11.1	6.8	8.7	4.5	7.9	3.6	15.8	
3	90	#12	-	-	6	3.4	-	-	-	-	25.8	8.7	-	-	-	-	5.7	3.5	-	
Median of G3 NET			23	15.8	9.8	5.9	8	5.5	9.2	5.3	10.8	8.7	15	9.6	8.7	4.5	8.6	4	13.2	

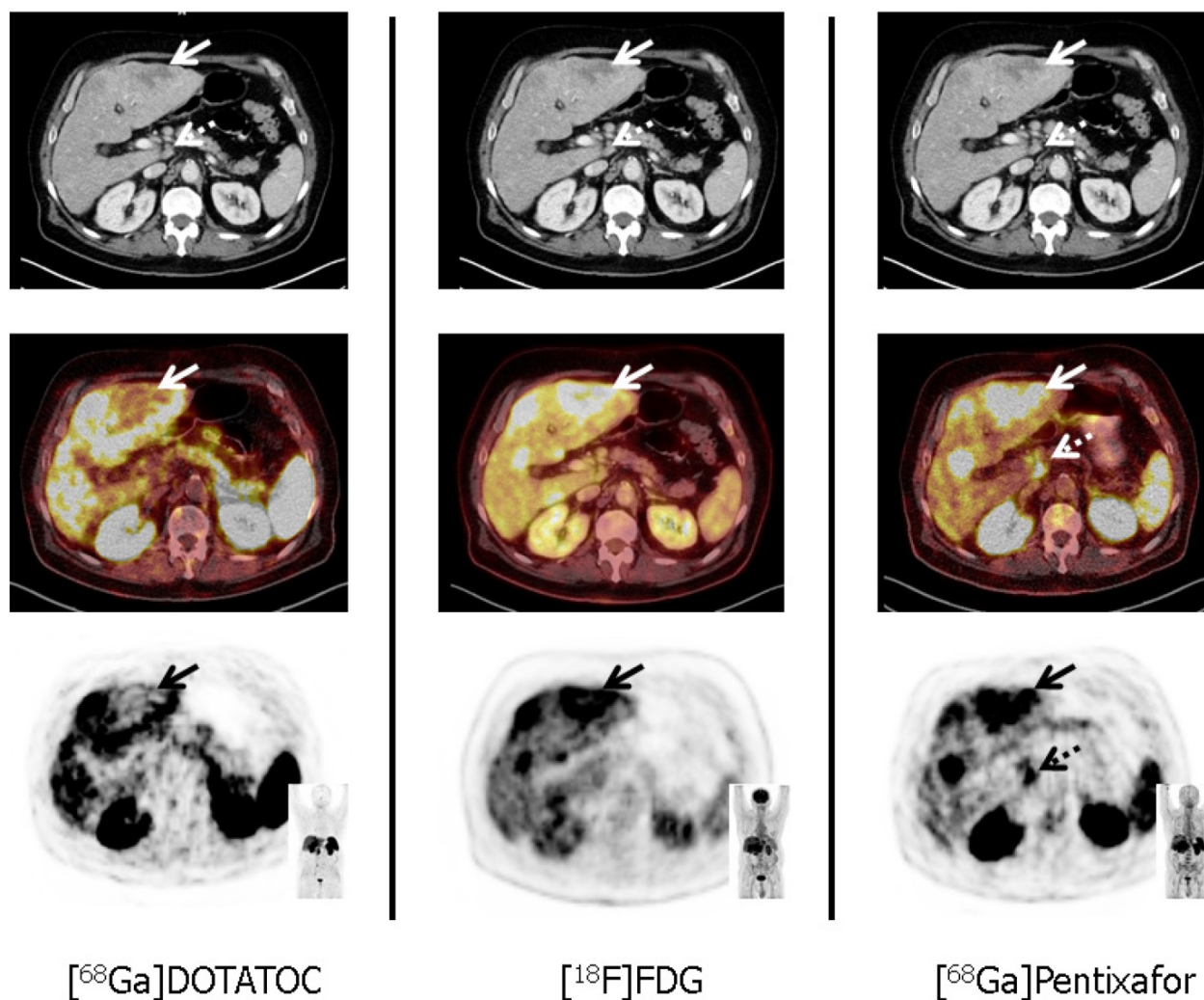


Figure 2. Tumor heterogeneity in a patient with a G3 gastric neuroendocrine tumor (NET) and liver metastases (patient #11; Ki67: 90%). In accordance with G3 NET, hypermetabolic hepatic metastases demonstrate loss of somatostatin receptor (SSTR) and up-regulation of CXCR4 expression (solid arrows, corresponding SUV_{max}: 10.3 for [⁶⁸Ga]Pentixafor, and 3.8 for [⁶⁸Ga]DOTATOC, respectively). Moreover, [⁶⁸Ga]Pentixafor provides additional information on disease extent by exclusively detecting a coeliac lymph node suspicious for metastatic disease (dotted arrows). All transaxial PET/(CT) images are displayed identically with a window level between 0 and 5.5. [⁶⁸Ga]DOTATOC = ⁶⁸Ga-DOTA-D-Phe-Tyr3-octreotide, [¹⁸F]FDG = ¹⁸F-fluorodeoxy-glucose.

Table 3. Heterogeneity of NET biology, as indicated by PET. In G1 NET, the vast majority of lesions showed sole expression of SSTR2, as indicated by focal retention of [⁶⁸Ga]DOTATOC (104 lesions), and only few (11 lesions) concurrent glucose use, as indicated by [¹⁸F]FDG-PET. No lesion was positive at [⁶⁸Ga]Pentixafor PET indicating no CXCR4 expression. In G3 NET, the vast majority of lesions revealed various combinations of SSTR and CXCR4 expression with or without deregulated glucose use.

G1 NET	[⁶⁸ Ga]DOTATOC	[¹⁸ F]FDG	[⁶⁸ Ga]Pentixafor
[⁶⁸ Ga]DOTATOC	104	11	0
[¹⁸ F]FDG	-	0	0
[⁶⁸ Ga]Pentixafor	-	-	0
G2 NET	[⁶⁸ Ga]DOTATOC	[¹⁸ F]FDG	[⁶⁸ Ga]Pentixafor
[⁶⁸ Ga]DOTATOC	107	10	3
[¹⁸ F]FDG	-	3	3
[⁶⁸ Ga]Pentixafor	-	-	0
G3 NET	[⁶⁸ Ga]DOTATOC	[¹⁸ F]FDG	[⁶⁸ Ga]Pentixafor
[⁶⁸ Ga]DOTATOC	0	11	12
[¹⁸ F]FDG	-	47	56
[⁶⁸ Ga]Pentixafor	-	-	9

Since some lesions were positive for all three tracers, the sum of lesions can exceed the number given in the manuscript. [⁶⁸Ga]DOTATOC = ⁶⁸Ga-DOTA-D-Phe-Tyr3-octreotide, [¹⁸F]FDG = ¹⁸F-fluorodeoxy-glucose.

[⁶⁸Ga]Pentixafor and [⁶⁸Ga]DOTATOC were concordantly positive in not more than 15 lesions (4 primary tumors, 9 LN, 1 bone and 1 liver lesion). 230 [⁶⁸Ga]DOTATOC-positive foci (1 primary tumor, 24 LN, 150 liver metastases, 50 bone metastases, 1 soft tissue metastasis and 4 peritoneal lesions) were missed by [⁶⁸Ga]Pentixafor; 54 lesions (1 primary tumor, 13 LN, 40 liver metastases) were CXCR4-positive and SSTR-negative.

In semi-quantitative analysis, [⁶⁸Ga]Pentixafor-PET-derived SUV and TBR were comparable to those calculated for [¹⁸F]FDG-PET. Corresponding individual values for all tracers are given in Table 2 and Supplementary Table 1.

Imaging results by tumor grade

G1 NET

All G1 NET (n=3) were [⁶⁸Ga]DOTATOC-positive and [⁶⁸Ga]Pentixafor-negative. [¹⁸F]FDG-PET yielded positive results in 2/3 patients. [⁶⁸Ga]DOTATOC-PET returned a total of 115 NET lesions (10 LN, 50 bone, 50 liver, 4 peritoneal, and 1 soft tissue metastases) as compared to 11 ([¹⁸F]FDG; 1 LN, 10 liver metastases) and 0 ([⁶⁸Ga]Pentixafor), respectively. [⁶⁸Ga]DOTATOC was the superior radiotracer in all cases. [⁶⁸Ga]Pentixafor did not yield additional or complementary information in any of those patients.

G2 NET

All G2 NET (n=4) were both SSTR- and [¹⁸F]FDG-positive, whereas CXCR4-positivity could only be observed in half of the cases (2/4). In parallel to G1 NET, [⁶⁸Ga]DOTATOC-PET revealed the highest number of sites of disease in all but one subject (patient #4) with a total of 118 lesions (3 primary tumors, 14 LN, 101 liver metastases), followed by [¹⁸F]FDG- (n=13; 2 primary tumors, 3 LN,

8 liver metastases) and [⁶⁸Ga]Pentixafor-PET (n=3; 2 primary tumors, 1 liver metastasis). [⁶⁸Ga]Pentixafor did not yield additional or complementary information in any patient.

G3 NET

Investigating G3 NET, 5/5 subjects were rated [¹⁸F]FDG positive. CXCR4- and SSTR-PET identified lesions in 4/5 patients each. On a lesion basis, [¹⁸F]FDG revealed the highest number of metastases in 3/5, [⁶⁸Ga]Pentixafor in the remaining 2/5 subjects. In total, [¹⁸F]FDG-PET detected 103 sites of disease (3 primary tumors, 56 LN, 1 bone, 43 liver metastases), followed by [⁶⁸Ga]Pentixafor- (n=66; 3 primary tumors, 22 LN, 1 bone, 40 liver metastases) and [⁶⁸Ga]DOTATOC-PET (n=12; 2 primary tumors, 9 LN, 1 bone metastasis).

The number of positive lesions for each PET tracer according to grading is given in Table 3.

Immunohistochemistry

Imaging results were compared to immunohistological staining for SSTR2a/5 and CXCR4 derived from biopsies of the primary tumor (n=8) or metastases (n=4). Regarding the histological evaluation of CXCR4 expression, 4/12 samples were rated "mild" (IRS 2, patient #4, #8, #9, and #11) and 1/12 "strongly" (IRS 9, patient #3, Figure 3) positive. Of note, relevant receptor expression on the cell surface could only be detected in 3 patients (patients #3, #8, #11), whereas CXCR4 was located intracytoplasmatic in the remaining 2 subjects. The remaining 7/12 samples (patients #1, 2, 5, 6, 7, 10, 12) were scored negative.

When imaging was performed, the site of histology was still present in 9/12 subjects (6 primary tumors [patients #3, #4, #6, #8, #9, #11], 3 liver metastases [patients #1, #2, #5]). [⁶⁸Ga]Pentixafor uptake of the respective lesion was substantially

corroborated by histology in 8/9 subjects (except patient #9 with an IRS of 1 and a negative [⁶⁸Ga]Pentixafor-PET). As a sign of intra-individual heterogeneity, whole-body imaging differed from sample-based immunohistological CXCR4 score as two patients with CXCR4-negative tumor samples (patients #2, #12) presented with -in patient-based analysis- positive [⁶⁸Ga]Pentixafor-PET scans. Interestingly, both subjects presented with

heterogeneous, rather low tracer uptake with a $SUV_{max} < 6.5$ (Figure 4).

In comparison, SSTR2a expression was rated “negative” in 4/12, “moderate” in 2/12 (patients #9, 10) and “strongly” positive in 6/12. SSTR5 was “mildly” positive in 3/12, “moderate” in 2/12 and “strongly” positive in 3/12 but negative in 4/12 (Table 1).

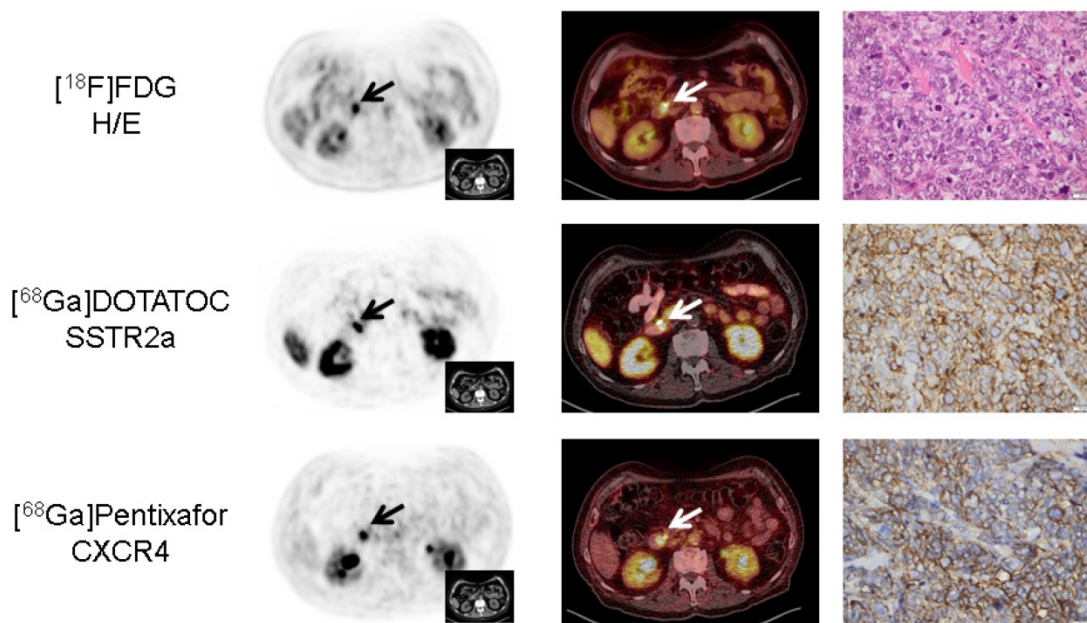


Figure 3. Concordance of immunohistochemistry and non-invasive receptor-directed PET imaging in a patient with pancreatic neuroendocrine tumor (NET; patient #3; Ki67: 85%). Display of transaxial PET (left) and fused PET/CT (middle) images of the primary tumor in the major pancreatic papilla (papilla of Vater; *papilla vateri*). The NET demonstrates high expression of both SSTR2a and CXCR4 which could be confirmed in the surgical specimen after tumor resection (right). Interestingly, CXCR4-PET correctly identified three additional lymph node metastases (versus none in [¹⁸F]FDG- and a single metastasis in SSTR-directed PET, Supplementary Figure 1). All PET/(CT) images are displayed identically with a window level between 0 and 5.5. [¹⁸F]FDG = ¹⁸F-fluorodeoxy-glucose, [⁶⁸Ga]DOTATOC = ⁶⁸Ga-DOTA-D-Phe-Tyr3-octreotide.

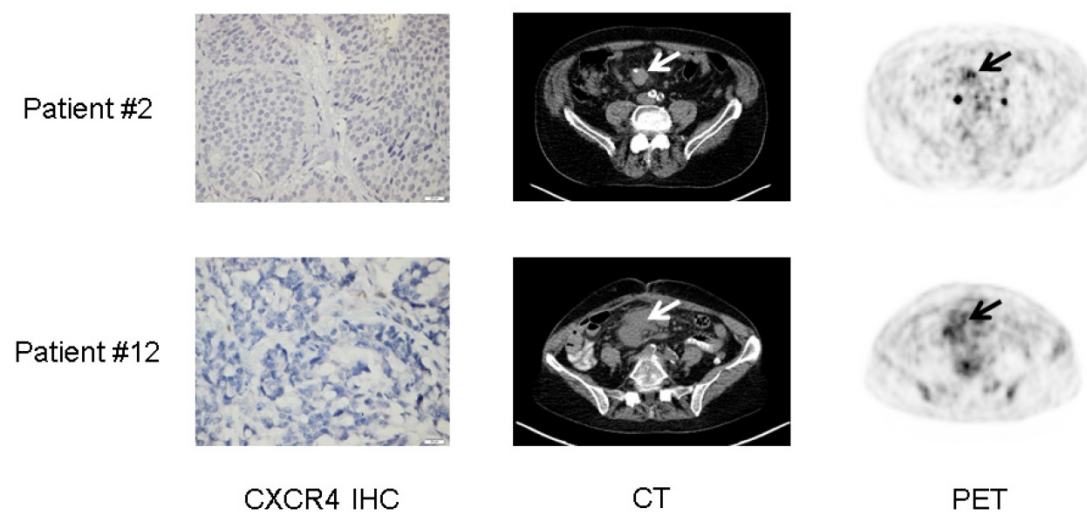


Figure 4. Lesional heterogeneity of CXCR4 expression in neuroendocrine tumor (NET). Display of 2 patients with G2 NET of the ileum (patient #2, Ki67: 10%) and G3 mixed adenoneuroendocrine carcinoma (MANEC, patient #12, Ki67: 90%), respectively. Both patients presented with negative immunohistochemistry (IHC) for CXCR4. As a possible explanation, [⁶⁸Ga]Pentixafor-PET imaging revealed very low, heterogeneous chemokine receptor expression (arrows) which might differ from the site of histology (liver and colon, respectively).

Discussion

This is the first report of non-invasive assessment of CXCR4 expression in GEP-NET. In the present cohort, CXCR4 expression could be visualized in patients with high-grade G3 neuroendocrine carcinomas. Of note, the majority of the [⁶⁸Ga]Pentixafor-positive subjects presented with highly proliferative disease with Ki67 of $\geq 85\%$, whereas well-differentiated tumors did not demonstrate relevant receptor expression on the cell surface.

[⁶⁸Ga]Pentixafor-PET findings could be corroborated by [¹⁸F]FDG-PET and somatostatin receptor PET imaging: Whereas all CXCR4-positive subjects also demonstrated high [¹⁸F]FDG uptake, SSTR expression as assessed by [⁶⁸Ga]DOTATOC was rather low or even absent.

These results are in line with a recent analysis of surgical GEP-NET samples reporting on an inverse expression of SSTR2 and CXCR4 in G1 to G3 NETs with an elevation in CXCR4 and a decrease in SSTR2a expression with increasing grade [10].

As expected, relevant SSTR expression could be mainly found in G1 and G2 NETs whereas most of the G3 NET lesions proved SSTR-negative. Whereas the recent NETTER-1 trial emphasized the paramount importance of peptide receptor radionuclide therapy for SSTR-positive tumors [6], molecular imaging or treatment with radiolabeled SSTR analogs is generally not useful for G3 tumors, which rarely express these receptors in an appropriate frequency and magnitude [7]. The mainstay of treatment for poorly differentiated NET consists of a platinum-based chemotherapeutic regimen which has proven high initial response rates of up to 80% [33]. However, as compared to small cell lung cancer, duration of response is rather limited with 8-11 months [34] and treatment options after failure of 1st-line chemotherapy are limited. Given the rather robust receptor expression in G3 NET, targeting of CXCR4 emerges as a promising new therapeutic approach for these patients. Recently, feasibility of CXCR4-directed ERT has been successfully demonstrated in the treatment of multiple myeloma and other hematologic malignancies [16]. Importantly, given the relevant hematotoxicity resulting in bone marrow ablation, autologous stem cell support is mandatory in all potential ERT candidates before therapy can be considered. Since most of the patients in whom CXCR4-directed ERT might become an option (G3 NET) receive hematotoxic standard chemotherapeutic regimens (platinum/etoposide) as first-line treatment, identification of sufficient receptor expression early in the course of treatment is essential in order not to

harm successful stem cell mobilization. However, if stem cells are available, ERT is easily performed and has been well-tolerated without any relevant further adverse effects [16].

Interestingly, distinct intra-individual tumor heterogeneity could be demonstrated in this cohort with the majority of patients displaying lesions with varying PET positivity. Whereas the notion of different patterns of [¹⁸F]FDG and [⁶⁸Ga]DOTATOC positivity is well-known and has been described in a number of studies [9, 35], the current project adds to the complexity of tumor biology: Whereas a relevant number of lesions with elevated glucose consumption did not overexpress CXCR4 on the cell surface, other lesions concordantly demonstrated [¹⁸F]FDG as well as chemokine receptor accumulation. This observation might be especially interesting for G2 NET patients in whom CXCR4 positivity might denote more aggressive disease.

On the other hand, tumor heterogeneity is an important factor when ERT eligibility is assessed. Since ERT will only be effective if (nearly) all lesions are addressed, pre-therapeutic comparison of [⁶⁸Ga]Pentixafor with [¹⁸F]FDG is mandatory not to miss a relevant subset of CXCR4-negative lesions.

The underlying mechanisms or prognostic value of those different lesions and how these lesions respond to current treatments has not been clarified yet. For a deeper understanding of the underlying biology, PET guided biopsies of lesions with divergent tracer uptake (and therefore different biology) will be performed at our center to gain additional insights into heterogeneity.

Further prospective studies also regarding the prognostic value of CXCR4-expressing disease in terms of therapy monitoring are highly warranted. Another unsolved question refers to potential synergistic combinations of various therapeutic agents and their effect on CXCR4 surface expression. Our group has experienced downregulation or loss of receptor shortly after initiation of anti-tumor therapy in small cell lung cancer patients [22]. Given the obvious pressure to start anti-tumor therapy in patients with advanced, highly aggressive disease, future studies will need to further investigate therapy-induced down- and, -preferably-, up-regulation of CXCR4. Potentially, a sequential combination with chemotherapeutic agents might lead to improved efficacy of CXCR4-directed ERT.

This study has several limitations. Because of the retrospective nature of the study, the statistical power is limited, also due to the relatively small sample size. Secondly, biopsies were not always obtained on a short-term period compared to the time point of PET imaging. Hence, correlation between histology and

imaging-derived receptor expression gives rise to significant bias, given the fact that receptor expression and functionality is subject to significant fluctuations. Additionally, histological confirmation of lesions with discordant tracer uptake (e.g. exclusive [⁶⁸Ga]Pentixafor uptake) to rule out false positive imaging results was not available in all cases. Finally, although a general agreement between histology and imaging could be demonstrated, [⁶⁸Ga]Pentixafor PET uptake seemed not to be corroborated by immunohistochemical findings in some cases. Of note, CXCR4 receptor expression is a dynamic process which can be influenced by a number of factors including therapies. [⁶⁸Ga]Pentixafor only addresses the receptors which are presented on the cell surface, whereas the cytoplasmatic or nucleic compartment cannot be addressed. Additionally, tumor biopsy samples are *per se* prone to sampling bias and cannot reflect the whole-body information derived by PET/CT imaging. Further studies to investigate down- and -preferably- up-regulation of CXCR4 are warranted.

Conclusion

Whereas CXCR4 expression seems to play only a limited role in well-differentiated NET, increasing receptor expression could be non-invasively observed with increasing tumor grade. Thus, [⁶⁸Ga]Pentixafor PET/CT might serve as non-invasive read-out for endoradiotherapy in advanced SSTR-negative, dedifferentiated tumors.

Supplementary Material

Supplementary figure and table.
<http://www.thno.org/v07p1489s1.pdf>

Acknowledgement

Parts of this work have been presented at the Annual Meeting of the Society of Nuclear Medicine and Molecular Imaging, 2016, San Diego, United States.

Competing Interests

HJW is the founder and shareholder of Scintomics. SK is CEO of Scintomics. This project has received funding from the Physician Scientist Training Program, CCC Mainfranken (AW). This project has received funding from the European Union's Horizon 2020 research and innovation programme under the Marie Skłodowska-Curie grant agreement (RAW). This publication was funded by the German Research Foundation (DFG) and the University of Wuerzburg in the funding programme Open Access Publishing. All other authors declare no conflict of interests.

References

1. Yao JC, Hassan M, Phan A, Dagohoy C, Leary C, Mares JE, et al. One hundred years after "carcinoid": epidemiology of and prognostic factors for neuroendocrine tumors in 35,825 cases in the United States. *J Clin Oncol.* 2008; 26: 3063-72.
2. Klimstra DS, Modlin IR, Coppola D, Lloyd RV, Suster S. The pathologic classification of neuroendocrine tumors: a review of nomenclature, grading, and staging systems. *Pancreas.* 2010; 39: 707-12.
3. Korse CM, Taal BG, van Velthuysen ML, Visser O. Incidence and survival of neuroendocrine tumours in the Netherlands according to histological grade: experience of two decades of cancer registry. *Eur J Cancer.* 2013; 49: 1975-83.
4. Saif MW. Lanreotide for the treatment of gastroenteropancreatic neuroendocrine tumors. *Expert Opin Pharmacother.* 2016; 17: 443-56.
5. Baum RP, Kluge AW, Kulkarni H, Schorr-Neufing U, Niepsch K, Bitterlich N, et al. [(177)Lu-DOTA](0)-D-Phe(1)-Tyr(3)-Octreotide ((177)Lu-DOTATOC) For Peptide Receptor Radiotherapy in Patients with Advanced Neuroendocrine Tumours: A Phase-II Study. *Theranostics.* 2016; 6: 501-10.
6. Strosberg J, El-Haddad G, Wolin E, Hendifar A, Yao J, Chasen B, et al. Phase 3 Trial of 177Lu-Dotatate for Midgut Neuroendocrine Tumors. *The New England journal of medicine.* 2017; 376: 125-35.
7. Ezziddin S, Attassi M, Yong-Hing CJ, Ahmadzadehfah H, Willinek W, Grunwald F, et al. Predictors of long-term outcome in patients with well-differentiated gastroenteropancreatic neuroendocrine tumors after peptide receptor radionuclide therapy with 177Lu-octreotate. *J Nucl Med.* 2014; 55: 183-90.
8. Modlin IM, Moss SF, Oberg K, Padbury R, Hicks RJ, Gustafsson BI, et al. Gastrointestinal neuroendocrine (carcinoid) tumours: current diagnosis and management. *Med J Aust.* 2010; 193: 46-52.
9. Basu S, Sirohi B, Shrikhande SV. Dual tracer imaging approach in assessing tumor biology and heterogeneity in neuroendocrine tumors: its correlation with tumor proliferation index and possible multifaceted implications for personalized clinical management decisions, with focus on PRRT. *Eur J Nucl Med Mol Imaging.* 2014; 41: 1492-6.
10. Kaemmerer D, Trager T, Hoffmeister M, Sipos B, Hommann M, Sanger J, et al. Inverse expression of somatostatin and CXCR4 chemokine receptors in gastroenteropancreatic neuroendocrine neoplasms of different malignancy. *Oncotarget.* 2015; 6: 27566-79.
11. Zlotnik A, Burkhardt AM, Homey B. Homeostatic chemokine receptors and organ-specific metastasis. *Nat Rev Immunol.* 2011; 11: 597-606.
12. Jacobson O, Weiss ID. CXCR4 chemokine receptor overview: biology, pathology and applications in imaging and therapy. *Theranostics.* 2013; 3: 1-2.
13. Gourni E, Demmer O, Schottelius M, D'Alessandria C, Schulz S, Dijkgraaf I, et al. PET of CXCR4 expression by a (68)Ga-labeled highly specific targeted contrast agent. *J Nucl Med.* 2011; 52: 1803-10.
14. Demmer O, Dijkgraaf I, Schumacher U, Marinelli L, Cosconati S, Gourni E, et al. Design, synthesis, and functionalization of dimeric peptides targeting chemokine receptor CXCR4. *J Med Chem.* 2011; 54: 7648-62.
15. Philipp-Abbrederis K, Herrmann K, Knop S, Schottelius M, Eiber M, Luckerath K, et al. In vivo molecular imaging of chemokine receptor CXCR4 expression in patients with advanced multiple myeloma. *EMBO molecular medicine.* 2015; 7: 477-87.
16. Herrmann K, Schottelius M, Lapa C, Osl T, Poschenrieder A, Hanscheid H, et al. First-in-Human Experience of CXCR4-Directed Endoradiotherapy with 177Lu- and 90Y-Labeled Pentixafor in Advanced-Stage Multiple Myeloma with Extensive Intra- and Extramedullary Disease. *J Nucl Med.* 2016; 57: 248-51.
17. Lapa C, Reiter T, Werner RA, Ertl G, Wester HJ, Buck AK, et al. [(68)Ga]Pentixafor-PET/CT for Imaging of Chemokine Receptor 4 Expression After Myocardial Infarction. *JACC Cardiovasc Imaging.* 2015; 8: 1466-8.
18. Herrmann K, Lapa C, Wester HJ, Schottelius M, Schiepers C, Eberlein U, et al. Biodistribution and radiation dosimetry for the chemokine receptor CXCR4-targeting probe 68Ga-pentixafor. *J Nucl Med.* 2015; 56: 410-6.
19. Wester HJ, Keller U, Schottelius M, Beer A, Philipp-Abbrederis K, Hoffmann F, et al. Disclosing the CXCR4 expression in lymphoproliferative diseases by targeted molecular imaging. *Theranostics.* 2015; 5: 618-30.
20. Lapa C, Luckerath K, Kleinlein I, Monoranu CM, Linsenmann T, Kessler AF, et al. (68)Ga-Pentixafor-PET/CT for Imaging of Chemokine Receptor 4 Expression in Glioblastoma. *Theranostics.* 2016; 6: 428-34.
21. Vag T, Gerngross C, Herhaus P, Eiber M, Philipp-Abbrederis K, Graner FP, et al. First Experience with Chemokine Receptor CXCR4-Targeted PET Imaging of Patients with Solid Cancers. *J Nucl Med.* 2016; 57: 741-6.
22. Lapa C, Luckerath K, Rudelius M, Schmid JS, Schoene A, Schirbel A, et al. [(68)Ga]Pentixafor-PET/CT for imaging of chemokine receptor 4 expression in small cell lung cancer--initial experience. *Oncotarget.* 2016; 7: 9288-95.
23. Lapa C, Schreder M, Schirbel A, Samnick S, Kortum KM, Herrmann K, et al. [(68)Ga]Pentixafor-PET/CT for imaging of chemokine receptor CXCR4 expression in multiple myeloma - Comparison to [18F]FDG and laboratory values. *Theranostics.* 2017; 7: 205-12.
24. Oken MM, Creech RH, Tormey DC, Horton J, Davis TE, McFadden ET, et al. Toxicity and response criteria of the Eastern Cooperative Oncology Group. *Am J Clin Oncol.* 1982; 5: 649-55.
25. Martin R, Juttler S, Muller M, Wester HJ. Cationic eluate pretreatment for automated synthesis of [(6)(8)Ga]CPCr4.2. *Nucl Med Biol.* 2014; 41: 84-9.

26. Boellaard R. Need for standardization of 18F-FDG PET/CT for treatment response assessments. *J Nucl Med.* 2011; 52 Suppl 2: 93S-100S.
27. Breeman WA, de Jong M, de Blois E, Bernard BF, Konijnenberg M, Krenning EP. Radiolabelling DOTA-peptides with 68Ga. *Eur J Nucl Med Mol Imaging.* 2005; 32: 478-85.
28. Kaemmerer D, Peter L, Lupp A, Schulz S, Sanger J, Baum RP, et al. Comparing of IRS and Her2 as immunohistochemical scoring schemes in gastroenteropancreatic neuroendocrine tumors. *Int J Clin Exp Pathol.* 2012; 5: 187-94.
29. Remmele W, Stegner HE. [Recommendation for uniform definition of an immunoreactive score (IRS) for immunohistochemical estrogen receptor detection (ER-ICA) in breast cancer tissue]. *Der Pathologe.* 1987; 8: 138-40.
30. Kloppel G, Couvelard A, Perren A, Komminoth P, McNicol AM, Nilsson O, et al. ENETS Consensus Guidelines for the Standards of Care in Neuroendocrine Tumors: towards a standardized approach to the diagnosis of gastroenteropancreatic neuroendocrine tumors and their prognostic stratification. *Neuroendocrinology.* 2009; 90: 162-6.
31. Kloppel G, Rindi G, Perren A, Komminoth P, Klimstra DS. The ENETS and AJCC/UICC TNM classifications of the neuroendocrine tumors of the gastrointestinal tract and the pancreas: a statement. *Virchows Arch.* 2010; 456: 595-7.
32. Rindi G, Arnold R, Bosman F. Nomenclature and classification of neuroendocrine neoplasms of the digestive system. In: Bosman FT, Carneiro F, Hruban RH, Theise ND, et al, editors WHO classification of tumors of the digestive system 2010; Lyon: IARC.
33. Ahlman H, Nilsson O, McNicol AM, Ruzsniowski P, Niederle B, Ricke J, et al. Poorly-differentiated endocrine carcinomas of midgut and hindgut origin. *Neuroendocrinology.* 2008; 87: 40-6.
34. Iwasa S, Morizane C, Okusaka T, Ueno H, Ikeda M, Kondo S, et al. Cisplatin and etoposide as first-line chemotherapy for poorly differentiated neuroendocrine carcinoma of the hepatobiliary tract and pancreas. *Japanese journal of clinical oncology.* 2010; 40: 313-8.
35. Basu S, Kwee TC, Gatenby R, Saboury B, Torigian DA, Alavi A. Evolving role of molecular imaging with PET in detecting and characterizing heterogeneity of cancer tissue at the primary and metastatic sites, a plausible explanation for failed attempts to cure malignant disorders. *Eur J Nucl Med Mol Imaging.* 2011; 38: 987-91.